BIOCHEMISTRY
including biophysical chemistry & molecular biology
Article

Biochemistry **2009,** *48,* 10591–10600 10591
DOI: 10.1021/bi901330g

Identification and Characterization of Binding Sites on S100A7, a Participant in Cancer and Inflammation Pathways†

Rafael León,‡ Jill I. Murray,‡ Gina Cragg,§ Benjamin Farnell,§ Nathan R. West,∥ Tamara C. S. Pace,‡ Peter H. Watson,∥ Cornelia Bohne,*,‡ Martin J. Boulanger,*,§ and Fraser Hof*,‡

‡*Department of Chemistry, University of Victoria, P.O. Box 3065, Victoria, British Columbia V8W 3V6, Canada,* §*Department of Biochemistry and Microbiology, University of Victoria, P.O. Box 3065, Victoria, British Columbia V8W 3V6, Canada, and* ∥*Deeley Research Centre, BC Cancer Agency, 2410 Lee Avenue, Victoria, British Columbia V8R 6V5, Canada*

Received July 31, 2009; Revised Manuscript Received October 7, 2009

ABSTRACT: S100A7 (psoriasin) is a member of the S100 family of signaling proteins. It is implicated in and considered a therapeutic target for inflammation and cancer, yet no small molecule ligands for S100A7 have been identified. To begin the development of specific small molecule inhibitors of S100A7 function, we have used a series of surface binding fluorescent dyes to probe the surface hydrophobic sites. Two naphthalene-based dyes (2,6-ANS and 1,8-ANS) were found to bind S100A7 in a distinct cleft. We characterized the binding interaction by determining both the structure of S100A7 bound to 2,6-ANS and the structure of S100A7 bound to 1,8-ANS to 1.6 Å. In both cases, two molecules of dye were docked such that the naphthalene groups were positioned in two symmetry-related grooves that are formed by the N-terminal helices of each monomer. We observed that Met12 acts as a gatekeeper to the binding cleft, adopting an "open" conformation for the more elongated 2,6-ANS while remaining in a "closed" conformation for the more compact 1,8-ANS. Steady-state fluorescence experiments revealed that S100A7 binds two copies of 2,6-ANS, each with a K_d of 125 μM. Time-resolved fluorescence lifetime measurements indicated that the two molecules of 2,6-ANS bind in two independent binding sites with different fluorescence lifetimes, suggesting that the S100A7 homodimer is not perfectly symmetric in solution. Isothermal titration calorimetry studies demonstrate that S100A7 has a higher affinity for 2,6-ANS than 1,8-ANS. Yeast two-hybrid studies were also used to probe contributions of individual residues of an S100A7 triple mutant with respect to Jab1 binding. Mutation of Leu78, which forms part of the Met12 cleft occupied by 2,6-ANS, reduced the level of Jab1 binding, suggesting a potentially important role for the Met12 hydrophobic pocket in defining a Jab1 interface. Additional Y2H studies also delineate contributions of Gln88 and in particular Asp56 that shows the most significant abrogated binding to Jab1. Collectively, these data suggest a complex interaction between S100A7 and the much larger Jab1. These studies form the basis for the development of small molecule reporters and modifiers of S100A7 form and function.

S100A7, also known as psoriasin, is a member of the S100 family of EF-hand calcium-binding signaling proteins. The S100 proteins are expressed exclusively in vertebrates and represent the largest subgroup within the superfamily of EF-hand Ca^{2+}-binding proteins (*1*). To date, more than 20 human S100 genes are known, of which 17 are tightly clustered in a region of the human 1q21 chromosome that is frequently rearranged in cancers (*2*−*4*).

S100A7 was first observed as a protein highly upregulated in lesions of psoriatic skin (*5*) and is considered to play a role in inflammation processes. It is upregulated and excreted from cells in the epidermis during inflammation and is a chemotactic factor for keratinocytes (*6*, *7*) and leukocytes (*8*). Its cell migration inducing properties are mediated by the receptor for advanced glycation end products (RAGE)[1] in a Zn^{2+}-dependent manner (*8*). In this extracellular context, S100A7 has also been implicated as a host-defense protein that selectively kills *Escherichia coli* on the surface of skin (*9*, *10*).

Within cells, S100A7 apparently lives a different life. Intracellular S100A7 expression is predominantly associated with squamous cell tumor subtypes in cancers of the lung, head and neck, cervix, and bladder (*11*−*14*). S100A7 has also been found to be expressed in nonsquamous tumors, including gastric cancer, melanoma, and breast cancer (*15*−*17*). S100A7 has been most heavily studied in breast tissue. Expression is absent or almost undetectable in normal breast epithelial cells. The frequency and

†F.H. and M.J.B. are Career Scholars of the Michael Smith Foundation for Health Research, and M.J.B. is supported by a CIHR New Investigator Award. This work was supported by the Canadian Breast Cancer Foundation and NSERC.

*To whom correspondence should be addressed. C.B. and F.H.: telephone, (250) 721-7193; fax, (250) 721-7147; e-mail, bohne@uvic.ca or fhof@uvic.ca. M.J.B.: telephone, (250) 721-7072; fax, (250) 721-8855; e-mail, mboulang@uvic.ca.

[1]Abbreviations: 1,8-ANS, 1-anilinonaphthalene-8-sulfonic acid; 2,6-ANS, 2-anilinonaphthalene-6-sulfonic acid; 3-AT, 3-aminotriazole; Bis-ANS, 4,4′-bis(1-anilinonaphthalene-8-sulfonate); DCIS, ductal carcinoma in situ; E-FABP, epidermal fatty acid binding protein; EGF, epidermal growth factor; EGFR, epidermal growth factor receptor; IRF, instrument response function; ITC, isothermal titration calorimetry; Jab1, c-Jun activation domain binding protein-1; MHC, major histocompatibility complex; PDB, Protein Data Bank; RAGE, receptor for advanced glycation end products; RanBPM, Ran-binding protein in the microtubule-organizing center; $S100A7_3$, S100A7 Asp56Gly/Leu78-Met/Gln88Lys triple mutant.

Published on Web 10/07/2009

level of expression increase in ductal carcinoma in situ (DCIS) lesions associated with an increasing risk of progression to invasive cancer; its highest level of expression is seen in high-grade DCIS, where it is among the most highly expressed proteins (*18*, *19*). Also, S100A7 expression correlates with increases in genes associated with MHC class II receptor activity, antigen processing and antigen presentation, and immune cell activation. These results are consistent with a role for S100A7 in modulating the immune response which may be a factor in early breast tumor progression (*20*).

S100 proteins are known in general to each have many interaction partners (*21*). The proteins for which direct interactions with S100A7 are described in the literature include RAGE (*8*), RanBPM (*22*), transglutaminase (*23*), and E-FABP (*24*, *25*). S100A7 also interacts with the signaling master regulator Jab1 (c-jun activation domain binding protein-1) (*26*). The formation of the S100A7−Jab1 complex is implicated in the development of early stage breast cancer (*27*). In breast cancer cells, the binding of S100A7 causes the regulatory protein Jab1 to translocate from the cytoplasm to the nucleus, where it stimulates a variety of downstream tumorigenic effects (*28*). Further, both S100A7 and Jab1 have been linked to the epidermal growth factor (EGF) and its tyrosine receptor kinase (EGFR), a pathway that contributes to a variety of cancers (*29*, *30*). Treatment of breast cells with EGF induces S100A7 expression, while down-regulation of S100A7 produces cells with reduced sensitivity to EGF-triggered angiogenesis and osteoclast formation. Further, treatment of breast cells with EGF causes translocation of Jab1 to the nucleus (the same effect that was previously observed upon treatment of cells with S100A7). Together, these results suggest that the S100A7−Jab1 complex is intimately connected to this well-known cancer/angiogenesis pathway. With a growing understanding of the dual roles of S100A7 as a mediator of disease-related cell migration (*6*−*8*, *31*) and cell growth (*29*, *30*) pathways, it has been proposed as a therapeutic target for the treatment of inflammation (*8*) and cancer (*27*, *28*, *32*).

The X-ray crystal structure of S100A7 has been determined at a resolution of 2.05 Å (*33*, *34*). S100A7 exists as a homodimer that binds two Ca^{2+} ions in EF-hand motifs and two Zn^{2+} ions at binding sites that span the dimer interface. In spite of this structural data and the wealth of data on biological functions and interaction partners, structural information on the participation of S100A7 in any of its complexes is scarce, and in some cases very crude: the triple mutation of putative Jab1-binding residues on S100A7 (Asp56Gly/Leu78Met/Gln88Lys) abrogates binding to Jab1 and eliminates all of the known downstream tumorigenic effects associated with S100A7 expression in breast cancer cells (*27*); the S100A7 homologue S100A15 (93% sequence identity, differing mainly in the C-terminal region) does not bind to RAGE in the same assays that confirmed S100A7's direct interaction with this receptor (*8*); an S100A7 mutant lacking N-terminal residues 1−34 and the C-terminal Zn^{2+}-binding motif (residues 81−101) is still active at killing *E. coli* (*10*).

No small molecule ligands for S100A7 are known, and very few ligand-binding sites on any S100 protein have been reported (*35*−*39*). We sought to probe the surface features of S100A7 that might give rise to binding of biological partners and potential therapeutic agents. To this end, we have studied the interaction of S100A7 with a collection of surface-binding fluorescent dyes. The fluorescence intensities of certain dyes are greatly affected by the mobility and polarity of their microenvironments (*40*), and several studies have used such dyes to identify surface hydrophobic sites on proteins (*41*−*44*). Time-resolved (lifetime) fluorescence studies are even more sensitive to fluorophore binding environments; they can discriminate between similar emissive species where the lifetime and intensity are altered by extremely subtle changes in the vicinity of the fluorophore (*45*, *46*).

We have identified a distinct binding site on the surface of S100A7 and characterized the molecular complexes of S100A7 with two isomeric dyes (2,6-ANS and 1,8-ANS) using X-ray crystallography, steady-state fluorescence, nanosecond time-resolved fluorescence, and isothermal titration calorimetry. These data instruct the studies of S100A7 in complex with its molecular partners and will guide the development of specific S100A7-binding small molecules for the study and modification of S100A7's numerous important biological functions.

EXPERIMENTAL PROCEDURES

Materials. Buffers and solutions were freshly prepared every day. 8-Anilinonaphthalene-1-sulfonic acid (1,8-ANS) and 6-anilinonaphthalene-2-sulfonic acid (2,6-ANS) were purchased from Invitrogen (Molecular Probes Inc.). These probes were used without further purification. All other reagents were of analytical grade.

Production and Purification of Soluble S100A7. Human S100A7 was amplified by PCR and cloned into the pET32a expression vector (Novagen) in frame with thioredoxin and an N-terminal hexahistidine tag. Recombinant expression of S100A7 was conducted in *E. coli* Rosetta-Gammi B (Invitrogen, Carlsbad, CA) grown in 2×YT media (DIFCO, Sparks, MD) supplemented with 50 μg/mL kanamycin (Sigma). The cells were grown at 37 °C to an OD_{600} of ∼0.8. The temperature was lowered to 30 °C. At an OD_{600} of 1, expression was induced with 0.75 mM isopropyl D-thiogalactoside (IPTG) for 8 h. The harvested cells were resuspended in 20 mM HEPES buffer (pH 8) with 20 mM imidazole and 500 mM NaCl (resuspension buffer) and lysed using a French press (SLM Instruments). The crude cell extract was centrifuged at 16000 rpm for 45 min to remove insoluble material and the supernatant applied directly to a Ni-NTA column (Qiagen) equilibrated with resuspension buffer. S100A7 fractions eluted with an increasing concentration of imidazole were analyzed via SDS−PAGE, pooled on the basis of purity, and concentrated. The S100A7 hexahistidine tag was proteolytically removed with thrombin (Novagen) and the protein purified on a SuperdexTM S-75 gel filtration column (Amersham Biosciences) equilibrated with 20 mM HEPES and 150 mM NaCl. The protein concentration was defined by amino acid analysis, by which an extinction coefficient ε_{280} of 57020 M^{-1} cm^{-1} was determined. A stock solution of 800 μM S100A7 was maintained at 4 °C. For each experiment, protein was diluted to a mother solution of 10 μM in buffer [40 mM Tris-HCl (pH 7.2), 100 mM KCl, and 2 mM $CaCl_2$] before being diluted to the final experimental conditions.

Crystallization, Data Collection, and Processing. Purified S100A7 was concentrated to 17 mg/mL and crystallized using the sitting drop vapor diffusion method at 18 °C in 0.2 M trisodium citrate and 0.1 M sodium cacodylate (pH 6.5). Crystals were soaked with either 2,6- or 1,8-anilinonaphthalenesulfonate (ANS) at a final concentration of 10 mM for 4 h and frozen at 100 K directly in the cryo stream. Diffraction data were collected on a Rigaku R-axis IV^{++} area detector coupled to an MM-002 X-ray generator with Osmic "blue" optics and an Oxford

Table 1: Data Collection and Refinement Statistics[a]

	2,6-ANS	1,8-ANS
Data Collection		
space group	$P4_32_12$	$P2_12_12_1$
a, b, c (Å)	51.66, 51.66, 117.24	51.60, 51.60, 116.91
α, β, γ (deg)	90, 90, 90	90, 90, 90
wavelength (Å)	0.9760	0.9760
resolution (Å)	47.30−1.70	47.21−1.70
no. of measured reflections	335832	479650
no. of unique reflections	18275	18199
redundancy	18.4 (15.7)	26.4 (22.5)
completeness (%)	99.9 (99.9)	100 (100)
$I/\sigma(I)$	33.2 (10.9)	34.1 (9.3)
R_{merge}[b]	0.068 (0.242)	0.072 (0.349)
Refinement		
R_{cryst}[c]/R_{free}[d]	0.182/0.210	0.188/0.212
no. of atoms		
protein	769	769
solvent	99	96
ligand	21	21
Ca^{2+}/Zn^{2+}	1/1	1/1
B values (Å^2)		
protein	16.08	14.47
solvent	27.47	27.14
ligand	28.32	13.48
Ca^{2+}/Zn^{2+}	12.38/12.98	10.45/12.63
root-mean-square deviation from ideality		
bond lengths (Å)	0.036	0.033
bond angles (deg)	2.753	2.563

[a]Values in parentheses are for the highest-resolution shell. [b]$R_{merge} = \sum_{hkl}|I - \langle I\rangle|/\sum_{hkl}I$, where I is the intensity of unique reflection hkl and $\langle I\rangle$ is the average over symmetry-related observations of unique reflection hkl. [c]$R_{cryst} = \sum|F_{obs} - F_{calc}|/\sum F_{fobs}$, where F_{obs} and F_{calc} are the observed and the calculated structure factors, respectively. [d]R_{free} is the R value using 5% of the reflections randomly chosen and omitted from refinement.

Cryostream 700 instrument. Diffraction data to 1.6 Å were processed using Crystal Clear with d*trek (*47*). Data collection and refinement statistics are listed in Table 1.

Structure Solution and Refinement. All refinement steps were conducted using the CCP4 suite of programs (*48*). Initial phases were obtained by molecular replacement (MR) using MOLREP (*49*) with the monomeric form of native S100A7 (PDB entry 2PSR) used as the search model. Solvent atoms were selected using COOT (*50*), and the overall structure was refined with REFMAC (*51*). Stereochemical analysis of the refined S100A7 structure was performed with PROCHECK and SFCHECK in CCP4 (*48*) with the Ramachandran plot showing excellent stereochemistry with more than 98% of the residues in the favored conformations for both structures and no residues modeled in disallowed orientations. Overall, 5% of the reflections were set aside for calculation of R_{free}. The coordinates for S100A7 in complex with 2,6- and 1,8-ANS have been deposited in the RCSB PDB as entries 2wos (structure factors, r2wosssf) and 2wor (structure factors, r2worsf), respectively.

Steady-State Fluorescence. Steady-state fluorescence spectra were recorded on a PTI QM-2 fluorimeter at 25 °C. The excitation wavelength was 319 nm, and spectra were collected between 350 and 600 nm. The excitation and emission slits were set with bandpasses of 3 and 6 nm, respectively. Fluorescence spectra were corrected for the baseline spectrum using a solution containing all compounds except ANS, ensuring that artifacts, such as Raman emission of the solvent and emission from the protein, were subtracted from the fluorescence spectra. The emission from the protein was < 1% of the fluorescence intensity for all solutions. Fluorescence intensities were determined by integrating the corrected spectra between 415 and 430 nm.

Fluorescence Binding Assays. Samples of 2,6-ANS (0.5 μM) and varying concentrations of S100A7 were prepared in 40 mM Tris (pH 7.2), 100 mM KCl, 2 mM $CaCl_2$ buffer, mixed gently by pipet, and incubated at room temperature for at least 30 min. Each sample was transferred to the cuvette by pipet and incubated in the fluorimeter, in the dark, for 10 min before the fluorescence scan was initiated. After the fluorescence scan was completed, the sample was incubated in the dark for 5 min and then a second fluorescence scan was initiated. Fluorescence spectra were recorded for each S100A7 concentration in the presence and absence of 2,6-ANS, as well as for controls of 2,6-ANS only and buffer only. The emission from ANS in buffer is less than 2% of the intensity from ANS at the lowest protein concentration examined. As this is smaller than the errors in the fluorescence measurements, the emission from ANS in buffer was not taken into account. The concentration of protein was calculated as the homodimer form, since this is the only species that has been observed in solution. The fluorescence spectra at each protein concentration were integrated, and the binding was analyzed assuming the equilibrium in eq 1, where the protein has n identical, independent binding sites for 2,6-ANS.

$$\mathrm{ANS} + n\mathrm{P} \rightleftarrows \mathrm{ANS{-}P} \quad (1)$$

This is equivalent to 1:1 binding between ANS and the protein, with the effective concentration of available protein binding sites being n[P]. S100A7 has two binding sites for 2,6-ANS (as determined by crystallography), and n was fixed to 2 for all fits. The binding isotherm (eq 2) can be derived from the definition of the equilibrium constant, and the mass balance equations (*52*):

$$\Delta I = \frac{F}{2}\left[K_d + nP_T + L_T - \sqrt{(K_d + nP_T + L_T)^2 - 4nP_TL_T}\right] \quad (2)$$

where K_d is the dissociation constant, P_T is the total protein concentration, L_T is the total ligand concentration, and F is a fluorescence scaling factor.

Assuming that the protein concentration is in excess of the ligand concentration, [P] $\sim$ P_T, and the following binding isotherm can be derived (eq 3).

$$\Delta I = \frac{\phi n P_T}{K_d + nP_T} \quad (3)$$

where ϕ is a fluorescence scaling factor. This equation can be linearized to give eq 4.

$$\frac{1}{\Delta I} = \frac{K_d}{\phi n P_T} + \frac{1}{\phi} \quad (4)$$

The equilibrium constant is determined from the curved plot (eq 2) as this results in the proper weighting of uncertainties. The linearity of the double-reciprocal plot (eq 4) supports the validity of the assumption that the binding sites are independent.

Experiments were also conducted with 2,6-ANS (from 0 to 100 μM) added to a constant concentration of S100A7 (1 μM) in

40 mM Tris-HCl, 100 mM KCl, and 2 mM $CaCl_2$ (pH 7.2). Following each addition of ANS, the solution was mixed and allowed to equilibrate for 30 min. For each solution of protein with ANS, a control solution of ANS alone in buffer was prepared.

Time-Resolved Fluorescence Measurements. Fluorescence decays were measured with an OB920 Edinburgh single-photon counter with a hydrogen flash lamp as the excitation source. The excitation and emission wavelengths were set to 319 and 423 nm, respectively, and the bandwidths for the excitation and emission monochromators were 16 nm. An iris was used to decrease, when necessary, the collection rate to less than 2.5% of the excitation rate. The number of counts in the channel of maximum intensity was 2000, and control experiments that included 10000 counts did not show any differences in the recovered values for the lifetimes and pre-exponential factors. All measurements were performed at 25 °C. A Ludox suspension was used to collect the instrument response function (IRF) at the excitation wavelength. The IRF was deconvoluted from the data in the fitting procedure using the Edinburgh software, and the decays were fit to a sum of exponentials (eq 5).

$$I_t = I_0 \sum_{1}^{i} (A_i e^{-t/\tau_i}) \quad (5)$$

where τ_i is the lifetime of each species and A_i the corresponding pre-exponential factor, where the sum of all pre-exponential factors is unity (eq 6).

$$\sum_{1}^{i} A_i = 1 \quad (6)$$

The values of χ^2 (0.9−1.1) and visual inspection of the residuals and autocorrelation were used to determine the quality of the fit (*53*).

Isothermal Titration Calorimetry. ITC measurements were taken using a VP-ITC calorimeter from MicroCal, LLC. S100A7 and ANS isomers were dissolved in 40 mM Tris-HCl, 100 mM KCl, and 2 mM $CaCl_2$ at final concentrations of 10 μM and 2 mM, respectively. The samples were degassed under vacuum prior to titrations. The reference cell was filled with Milli-Q water. The titration of S100A7 with 1,8-ANS and 2,6-ANS involved 28 injections of ligand solution (the first injection was 2 μL, and all remaining injections were 10 μL). In all cases, the ligand solution was injected at 4 min intervals. The syringe stirring speed as set at 307 rpm, and the temperature of the titration cell was set at 30 °C. The heat of ligand dilution in buffer, determined in separate experiments, was subtracted from the titration data. Raw data were integrated and processed with Origin 7.0 provided by the manufacturer. The first injection in each experiment was not taken into account for the analysis. Three independent experiments with 2,6-ANS and two independent experiments with 1,8-ANS were analyzed separately.

Yeast Two-Hybrid Assays. For yeast two-hybrid studies, amino acids 42−335 of human Jab1 were expressed as a fusion with the GAL4 DNA binding domain in bait plasmid pGBT9 (Clontech). Wild-type or mutant S100A7 (generated through PCR mutagenesis) was expressed as a fusion with the GAL4 activation domain in prey plasmid pACT2.2 (Addgene plasmid 11343, deposited by G. Caldwell). *Saccharomyces cerevisiae* strain Y190 (ATCC) was cotransformed with each construct using the lithium acetate method (*54*). Relative S100A7−Jab1 interaction strength was assessed by plating transformed cells onto selective medium lacking leucine, tryptophan, and histidine (Sigma) with various concentrations (10, 25, or 50 mM) of the histidine analogue 3-aminotriazole (3-AT), or onto leucine/tryptophan deficient control plates. Colony formation on selective relative to control medium was assessed in triplicate after approximately 1 week. Differences were assessed using a Student's *t* test.

RESULTS

S100A7 was produced in *E. coli* as a soluble protein and purified to homogeneity. Analysis using gel filtration chromatography showed that S100A7 existed as a stable dimer consistent with previous reports (*33*). S100A7 crystallized with one monomer in the asymmetric unit of the tetragonal unit cell with the second molecule of the physiological dimer generated by the crystallographic 2-fold axis. Crystals of S100A7 were soaked with a variety of probe molecules, including Nile Red, Bis-ANS, 2,6-ANS, and 1,8-ANS, and were re-examined via X-ray diffraction. Only crystals treated with 2,6-ANS and 1,8-ANS gave new density indicative of binding under these conditions. S100A7 costructures with each ANS isomer were refined to a final resolution of 1.6 Å with the final models starting at Ser1 and extending through Ser96 (Figure 1). Each S100A7 monomer coordinates one Ca^{2+} ion and contributes two of the four ligands to the coordination of each of the two Zn^{2+} ions bound at the homodimer interface. Both S100A7−ANS costructures exhibit unambiguous electron density for the protein backbone and bound dye molecules with low temperature factors and excellent stereochemistry, with more than 98% of the residues adopting the most favorable conformation and no residues in the disallowed conformation. Final data collection and refinement statistics are presented in Table 1.

The S100A7 Ca^{2+} ions in the 2,6- and 1,8-ANS costructures deviate less than 0.25 $Å^2$ [root-mean-square deviation (rmsd)] from the previously reported native S100A7 structure (*34*), indicating the binding of the dyes does not significantly perturb the monomer fold or homodimer structure. Both 2,6- and 1,8-ANS dock into the same groove on S100A7 formed by the N-terminal helices of each monomer. The binding of the more elongated 2,6-ANS isomer results in a side chain conformational change in which the aniline ring displaces the side chain of Met12 by more than 5 Å such that it adopts an "open" conformation. The gatekeeper Met12 side chain swings back into the spacious neighboring Leu78 pocket and opens its own pocket to accommodate the incoming small molecule, all without significant movement by any other neighboring residues. The naphthalene group of 2,6-ANS is positioned directly between the N-terminal helices and packs against Gly11 from one monomer and Ala5 and Ser8 from the second monomer. The sulfonate group is directed away from S100A7 toward solvent and is stabilized through interactions with the side chain of Gln4. A comparison of the 2,6- and 1,8-ANS costructures reveals that the naphthalene groups of the two dye molecules adopt similar orientations between the N-terminal helices. The more compact structure of the 1,8-ANS isomer, however, results in the aniline group being directed away from the core of the dimer interface. As a result, the side chain of Met12 is not displaced and instead adopts the "closed" position observed in the native S100A7 structure. The side chain Lys18 on the surface of S100A7 is, however, displaced by ~3.4 Å to accommodate the aniline group of 1,8-ANS.

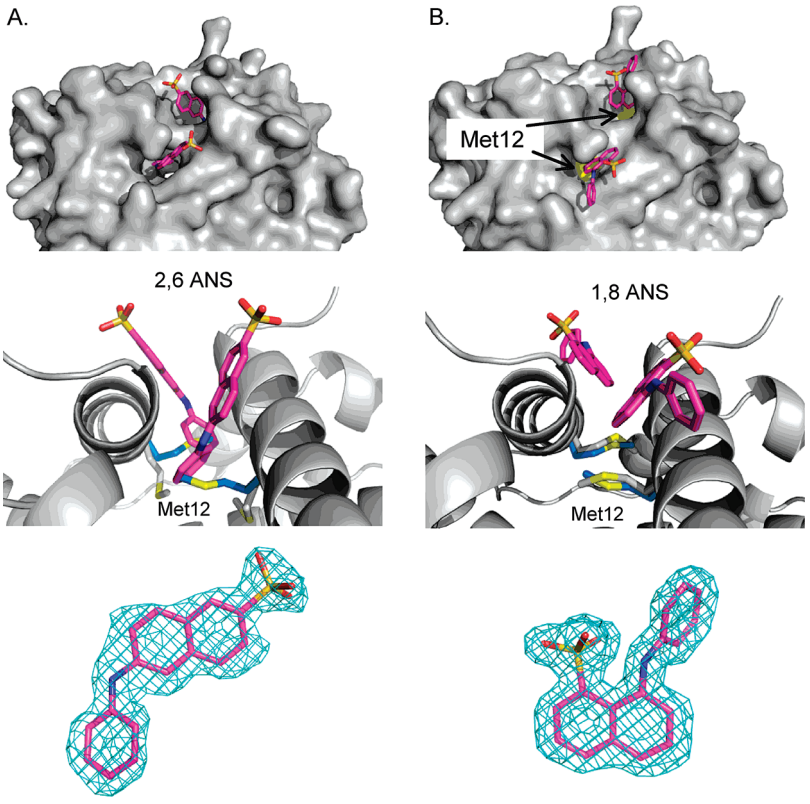

FIGURE 1: Probing surface pockets of S100A7 with isomers of ANS. Cartoon representation of the symmetry-calculated dimer of S100A7 in complex with (A) 2,6-ANS and (B) 1,8-ANS. Binding of 2,6-ANS to S100A7 displaces the side chain of Met12 (gray) relative to the position adopted in the native structure (blue), exposing a deep tunnel that spans the S100A7 dimer. The 1,8-ANS, however, does not penetrate as deeply into S100A7 and as a result does not displace the side chain of Met12. The $2F_o - F_c$ electron density maps of 2,6- and 1,8-ANS calculated at 1.2σ are shown in the bottom left and right panels, respectively.

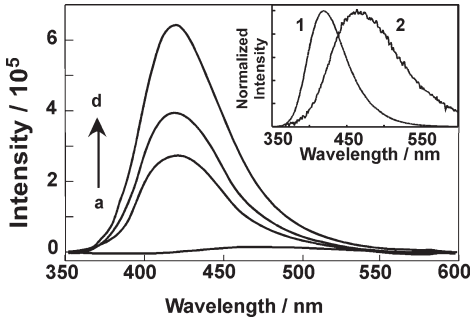

FIGURE 2: Fluorescence spectra (λ_{ex} = 319 nm) of 0.5 μM 2,6-ANS in the presence of increasing concentrations of S100A7: (a) 0, (b) 30, (c) 50, and (d) 250 μM. The inset shows normalized fluorescence spectra of 2,6-ANS (0.5 μM) bound to 250 μM S100A7 (1) and in buffer (2). Buffer consisted of 40 mM Tris-HCl, 100 mM KCl, and 2 mM $CaCl_2$ (pH 7.2) at 25 °C.

The solution binding of 1,8-ANS and 2,6-ANS to S100A7 was studied using steady-state and time-resolved fluorescence experiments. Both isomers of ANS are weakly fluorescent in aqueous solution, while fluorescence is enhanced when they are located in a constrained environment. Titration of S100A7 (1 μM) with 1,8-ANS did not result in any observable increase in the fluorescence emission of the dye, up to a concentration of 100 μM, and no further fluorescence studies were conducted with 1,8-ANS. A similar lack of response was also observed for Bis-ANS and Nile Red. Titration of S100A7 (1 μM) with the 2,6-ANS isomer resulted in fluorescence enhancement relative to free 2,6-ANS, which is indicative of binding (Figure 2). The increase in fluorescence intensity was accompanied by a blue shift of 40 nm, a result typical of an ANS dye bound in a nonpolar environment (*45*). S100A7 contains no Trp residues, and thus, the inherent protein fluorescence is insignificant under these experimental conditions.

At a constant concentration of S100A7 (1 μM), the 2,6-ANS fluorescence emission intensity ($I - I_0$) increased throughout the titration with 2,6-ANS (from 0 to 100 μM). The plot of $I - I_0$ versus ANS concentration is sigmoidal and does not level off at higher ANS concentrations (Figure 3A). This is indicative of binding to additional weaker sites at the higher ANS:protein ratios, and this protocol is not suitable for recovery of K_d for the higher-affinity ANS binding sites. In addition, at high concentrations of ANS, the absorbance at the excitation wavelength is high, and there is no longer a linear relationship between fluorescence intensity and concentration.

Under conditions where there is an excess of S100A7, 2,6-ANS should selectively bind to the highest-affinity sites available, and the changes observed in the fluorescence intensities can be attributed to binding at these sites. Addition of S100A7 (from 0 to 250 μM) to a constant 2,6-ANS concentration (0.5 μM) was conducted. As the amount of protein was increased, the fluorescence intensity increased and a blue shift in the emission maximum was again observed. A K_d of 125 ± 11 μM was recovered from the nonlinear fit of the fluorescence intensity to eq 2 when the number of independent binding sites is fixed to 2 (Figure 3B). The double-reciprocal plot for the data (Figure 3C) was linear, indicating that the assumption of independent sites was reasonable and that the K_d values for these two sites are similar.

Steady-state fluorescence spectra are a sum of the contributions from each emissive species in solution. Time-resolved

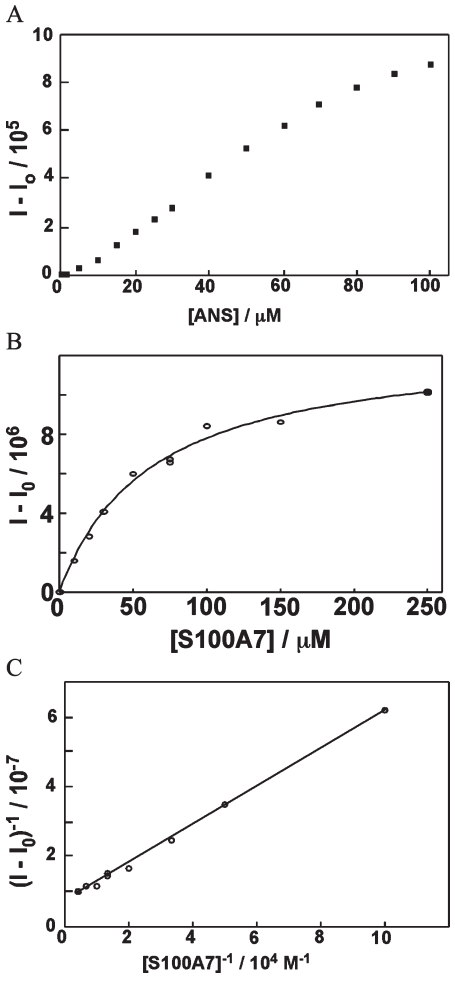

FIGURE 3: (A) Fluorescence titration of S100A7 (1 μM) by S100A7 ($I - I_0$; λ_{ex} = 319 nm, and λ_{em} = 423 nm). (B) Fluorescence titration of 2,6-ANS (0.5 μM) by S100A7 ($I - I_0$; λ_{ex} = 319 nm, and λ_{em} = 415−430 nm). The solid line is the result of the fitting of the data to eq 2, where the number of independent binding sites was fixed to 2. (C) Double-reciprocal plot for the data from the fluorescence titration of 2,6-ANS (0.5 μM) by S100A7 ($I - I_0$; λ_{ex} = 319 nm, and λ_{em} = 415−430 nm). The solid line is the result of the fitting of the data to eq 4.

studies, however, can differentiate fluorophores that have the same emission spectra but different emission efficiencies, i.e., lifetimes. Time-resolved fluorescence experiments were conducted to determine the fluorescence lifetimes of 2,6-ANS under conditions similar to those used in steady-state fluorescence experiments. For 2,6-ANS in the presence of S100A7, all lifetime decays were fitted to a sum of exponentials (eq 5).

2,6-ANS is short-lived in buffer, and a lifetime of 0.47 ns was recovered. This is slightly longer than what has been reported previously (0.35 ns) (*55*), but this is probably due to poor resolution for deconvolution of shorter lifetimes from the IRF in our experimental setup. This lifetime was fixed for all further fits where free 2,6-ANS was present in solution. To obtain the lifetime of S100A7-bound 2,6-ANS, fluorescence decays were obtained under conditions with excess fluorophore, to saturate protein binding ([S100A7] = 1 μM, and [2,6-ANS] = 5−100 μM). Surprisingly, in the presence of protein, there were two lifetimes in addition to that for ANS in buffer, and the fluorescence decays were adequately fit to a sum of three exponentials. When the lifetime for 2,6-ANS in buffer was fixed to 0.47 ns, the two additional lifetimes remained constant, with average values

Table 2: 2,6-ANS Fluorescence Decay Parameters at Various 2,6-ANS Concentrations with a Constant Concentration of S100A7 (1 μM) Recovered from the Fit of the Data to a Sum of Three Exponentials[a]

[ANS] (μM)	A_1 (τ_1 = 10.7 ns)	A_2 (τ_2 = 5.08 ns)	A_3 (τ_3 = 0.47 ns)	χ^2
5	0.14	0.12	0.74	1.024
10	0.16	0.14	0.70	1.029
15	0.15	0.13	0.72	0.953
20	0.15	0.13	0.73	0.976
25	0.13	0.11	0.76	0.953
30	0.17	0.11	0.72	0.957
40	0.15	0.13	0.72	0.972
50	0.16	0.12	0.72	0.992
60	0.13	0.13	0.74	0.948
70	0.11	0.11	0.78	1.009
80	0.10	0.10	0.82	0.987
90	0.11	0.10	0.79	0.992
100	0.11	0.10	0.80	0.969

[a]The lifetimes for each exponential were kept constant with respect to the average values recovered from fits in which all parameters were free. Intensity was recorded at a λ_{ex} of 319 nm and a λ_{em} of 423 nm. Buffer consisted of 40 mM Tris-HCl, 100 mM KCl, and 2 mM $CaCl_2$ (pH 7.2). The errors for the A values are ±0.02.

Table 3: 2,6-ANS Fluorescence Decay Parameters at Various S100A7 Concentrations with a Constant Concentration of 2,6-ANS (0.5 μM) Recovered from the Fit of the Data to a Sum of Two Exponentials[a]

[S100A7] (μM)	A_1 (τ_1 = 10.7 ns)	A_2 (τ_2 = 5.08 ns)	χ^2
10	0.49	0.51	1.161
30	0.50	0.50	1.092
50	0.50	0.50	1.370
75	0.49	0.51	1.086
100	0.53	0.47	0.994
250	0.46	0.54	1.006

[a]The lifetimes for each exponential were kept constant with respect to the average values recovered from fits in which all parameters were free. Intensity was recorded at a λ_{ex} of 319 nm and a λ_{em} of 423 nm. Buffer consisted of 40 mM Tris-HCl, 100 mM KCl, and 2 mM $CaCl_2$ (pH 7.2). The errors for the A values are ±0.02.

of 10.7 and 5.08 ns. This means there are three environments experienced by ANS: one environment in bulk solution and the other two protein-bound.

The pre-exponential factor (A_i) for each species is related to its concentration, taking into account the species' excitation efficiency. The excitation efficiencies are unknown; however, trends in the A_i values can be correlated to changes in concentration. Changes in the A_i values with changes in the 2,6-ANS or S100A7 concentration can be diagnostic for species with different binding efficiencies. If, at a constant protein concentration, one binding site has a higher affinity than the other, this site would be occupied first, and occupancy of the second weaker site would occur only as the concentration of ligand was increased. This would be reflected as an increase in the A_i value for one of the protein-bound ANS species relative to the A_i value for the second protein-bound species. To decrease errors in the A_i values, the fluorescence decays were fit with lifetimes held constant at 10.7, 5.08, and 0.47 ns (Table 2). As the concentration of 2,6-ANS is increased, the A_3 value for ANS in water increases somewhat, while the A_1 and A_2 values for protein-bound ANS decrease slightly. However, the A_1/A_2 ratio is constant and equal to 1.2 ± 0.2, indicating that the two protein sites on which they report are equally populated and therefore must have similar binding

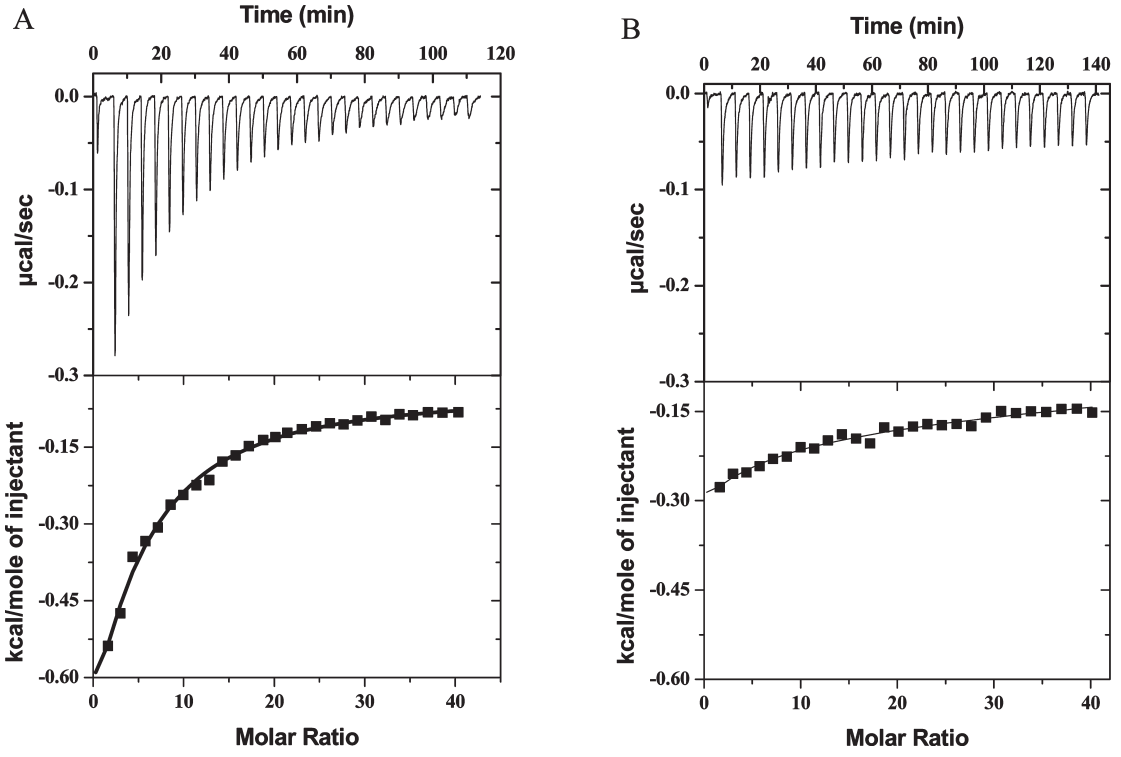

FIGURE 4: Isothermal titration calorimetry (ITC) data for titration of (A) 2,6-ANS and (B) 1,8-ANS into a solution of S100A7. The S100A7 concentration in the cell was 10 μM; the syringe concentrations of 2,6-ANS and 1,8-ANS were 2 mM. The top panel of each figure shows raw titration data arising from 10 μL injections, while the bottom panel shows integrated heats of binding for each injection point corrected for heats of dissolution determined in separate experiments (not shown). Unique fitting solutions could not be determined.

constants. The additional weak binding of 2,6-ANS to S100A7 observed in the steady-state studies under these conditions is not apparent in the time-resolved studies. This is most likely because the increase in the lifetime of 2,6-ANS in these weak binding sites is minimal and the population of these sites is small.

Experiments conducted with excess protein ([2,6-ANS] = 0.5 μM, and [S100A7] = 10−250 μM) yielded results similar to those with excess fluorophore. Under these conditions, there is no contribution to the decay from ANS in buffer, indicating that all ANS is bound, and all the fluorescence decays were adequately fit to the sum of two exponentials. The two lifetimes recovered were similar to the lifetimes of 10.7 and 5.08 ns observed above, demonstrating that the same binding sites are occupied under both sets of conditions. To decrease errors in the recovered A_i values, fits were performed where these two lifetimes were held constant (Table 3). There were no changes in the A values as the protein concentration was increased, and the A_1/A_2 ratio was constant at 0.9 ± 0.1, indicating again that the populations of these two protein-bound species are equal and that they must have similar association constants for the protein.

Because of the lack of fluorescence enhancement from bound 1,8-ANS, we used isothermal titration calorimetry (ITC) to compare the binding of the two ANS isomers to S100A7. Isolation of higher-affinity sites by inverse titration of S100A7 into 2,6-ANS was impossible because of the prohibitive amount of protein required for such ITC measurements. Instead, titration of solutions of each ANS isomer (2 mM) into S100A7 (10 μM) was conducted at 30 °C. Each injection of 1,8-ANS into S100A7 gave slightly exothermic peaks and little curvature, suggestive of very weak binding (Figure 4B). The titration of 2,6-ANS into S100A7 under identical conditions gives larger exotherms and greater curvature (Figure 4A). Fitting the multiple parameters (K_{assoc}, ΔH, ΔS, and stoichiometry n) to unique solutions was impossible in both cases, as expected for the multiple higher- and lower-affinity binding sites that are engaged during these ANS-into-protein titrations. Nevertheless, we can conclude from these ITC data that 2,6-ANS binds to S100A7 with a more negative ΔH and a higher affinity versus those of 1,8-ANS.

S100A7 exerts tumorigenic effects in breast cells through an interaction with Jab1 that can be abrogated upon mutation of three residues (Asp56Gly, Leu78Met, and Gln88Lys), known as the S100A7 triple mutant ($S100A7_3$) (*27*). The triple mutant has been extensively studied in engineered cancer cells lines and using the yeast two-hybrid assay (*27*). However, the impact of each individual mutation has not been assessed. Of particular interest is Leu78, which lies directly adjacent to the ANS binding site. To assess the effect of each mutation individually, especially Leu78-Met, we produced three singly mutated S100A7 clones for use in a yeast two-hybrid assay with Jab1, in addition to wild-type and triple mutant S100A7. We observed that each single mutation was sufficient to abrogate yeast growth on selective medium (Figure 5), revealing each of the three mutations (Asp56Gly, Leu78Met, and Gln88Lys) is detrimental to Jab1 interaction. The use of progressively more stringent selection conditions (increasing concentrations of 3-AT) allows the ranking of the effect at each residue, in the following order: Asp56 > Leu78 > Gln88 (Figure 5).

DISCUSSION

X-ray cocrystal structures reveal that both 2,6-ANS and 1,8-ANS bind at the same Met12 cleft in S100A7 (Figure 1), while treatments with bis-ANS or Nile Red did not result in the observation of any bound dye at the Met12 pocket or at any other surface site on the protein. Solution studies with the two larger dyes also show no fluorescence enhancement, suggesting

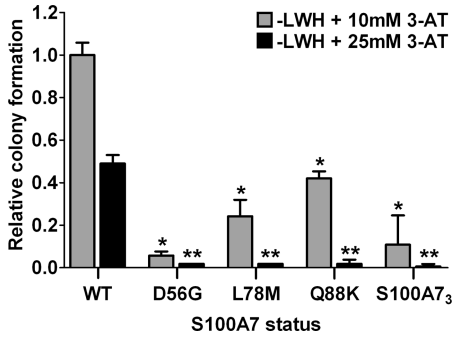

FIGURE 5: Leu78, Asp56, and Gln88 are each necessary for interaction of S100A7 with its ligand Jab1. Yeast strain Y190 was transformed with Jab1-pGBT9 (bait) and wild-type or mutant S100A7-pACT2.2 (prey) plasmids. Transformants were plated onto leucine/tryptophan/histidine-deficient medium containing 10, 25, or 50 mM 3-aminotriazole (3-AT) to allow increasing strengths of selection. Colonies were counted after 1 week and normalized to growth on leucine/tryptophan-deficient control plates. Data shown represent colony formation relative to clones transformed with wild-type S100A7. No cells grew on media with 50 mM 3-AT, and thus, these data are not shown. Bars represent means of triplicate assays ± the standard deviation. *$P < 0.001$ and **$P < 0.0001$ relative to wild-type transformants under same selection conditions, based on a Student's t test.

that they are not bound in solution or in the solid state. Both 1,8-ANS and 2,6-ANS adopt curved conformations upon binding, explaining the rejection of the longer and more rigid bis-ANS and Nile Red dyes from the deep and narrow Met12 pocket.

Solution studies also reveal no fluorescence enhancement for 1,8-ANS, a molecule whose binding-induced fluorescence has been used extensively to characterize binding sites in proteins (*55*−*57*). This lack of fluorescence enhancement, which runs contrary to the binding observed in the solid state, can be explained on the basis of the crystal structure: the aniline ring of bound 1,8-ANS is fully exposed to solution and free to rotate about its C−N bonds, and as such, 1,8-ANS does not experience the restricted, nonpolar environment that is normally required for enhancement of emission. The ITC data reveal clearly that 1,8-ANS binding is weaker than that observed for 2,6-ANS. Although both solution-phase studies show that the affinity of 1,8-ANS for S100A7 must be very low, its appearance at the Met12 cleft in the X-ray structure suggests that this location is one of the most hydrophobic sites on the surface of S100A7. Indeed, while 1,8-ANS makes extensive hydrophobic contacts between its naphthalene ring and neighboring side chains, the only polar contacts observed in the structure are two solvent-exposed hydrogen bonds between the sulfonate of 1,8-ANS and Gln4.

The binding of 2,6-ANS differs markedly from that of 1,8-ANS in both solution and the solid state. 2,6-ANS is known to associate weakly with multiple protein sites (*56*), and the steady-state fluorescence data obtained in the presence of excess fluorophore (Figure 3A) suggest that it can indeed bind to multiple low-affinity sites on S100A7 that provide some degree of fluorescence enhancement. However, only two molecules of 2,6-ANS are observed in the cocrystal structure, and both are deeply buried in the Met12 cleft. Under conditions in which S100A7 is in excess relative to 2,6-ANS, the fluorescent binding partner is able to choose and occupy only the highest-affinity binding sites. Thus, the data arising from inverse titrations of protein into 2,6-ANS allow isolation of the binding constant of the highest-affinity sites.

A K_d of 125 ± 11 μM was recovered from the fit of the steady-state fluorescence when the assumption of two binding sites per S100A7 homodimer was made. Time-resolved studies show two distinct protein-bound 2,6-ANS species. The ratio of the populations of these two species does not change with the concentration of S100A7 or 2,6-ANS, indicating that the dissociation constant for each species is the same. However, as the lifetimes of these two species are different, the environments surrounding the fluorophore are not identical.

The crystal structure shows that two molecules of 2,6-ANS are bound in the two symmetry-related Met12 clefts of the S100A7 homodimer. However, the two copies of bound 2,6-ANS are symmetrically disposed in the crystal structure, and such an arrangement must give rise to identical excited-state lifetimes for each. How can we explain the consistent observation that each molecule of bound 2,6-ANS exhibits a different excited-state lifetime under the large range of conditions studied? It is possible that in solution the different environments for each copy of 2,6-ANS arise from differing conformations of the two bound copies of 2,6-ANS within a perfectly symmetric S100A7 dimer. An alternative explanation arises if one considers that S100A7 consistently exists in solution as a homodimer with broken symmetry. Indeed, S100A7 was previously reported to crystallize as a nonsymmetric dimer in the presence of low Zn^{2+} concentrations, and that structure reveals striking dissymmetry in the Met12 region (*34*). It is possible that a similar nonsymmetric structure of S100A7 is significantly populated in solution. Whatever the structural explanation, the use of time-resolved fluorescence here reveals a loss of symmetry for the S100A7−2,6-ANS complex in solution that is invisible to steady-state fluorescence titrations, X-ray crystallography, and ITC.

One of the two Met12 clefts is open in structure 3PSR (*34*). Both are closed in structures 1PSR and 2PSR (*33*, *34*). Both are partially open in the 1,8-ANS costructure determined here. Both are completely open and engaged in the presence of 2,6-ANS. Is it a physiologically relevant binding site? No functional recombinant Jab1 exists, so direct in vitro studies of S100A7 interaction sites are impossible; however, several indirect lines of evidence support the relevance of the Met12 binding cleft to the functions of S100A7. The binding of both ANS isomers in the same Met12 cleft suggests that this surface patch has the hydrophobic character typical of protein−protein interaction sites. Further support for the physiological relevance of the Met12 binding site is given by examination of the only S100A7 mutations that have been shown to impact directly a protein−protein interaction of S100A7. The S100A7−Jab1 interaction and its downstream signaling effects are abolished upon mutation of Gln88, Asp56, and Leu78. The S100A7 triple mutant, S100A7$_3$, has been previously shown to abrogate Jab1 binding in yeast-two hybrid screens and to shut down completely the S100A7-induced carcinogenic effects in cell-based and xenograft studies of breast cancer (*27*). We have also recently shown that the triple mutant remains folded in the solid state (rmsd of Cα atoms of 0.79 Å relative to the wild type), remains fully loaded with Ca^{2+} and Zn^{2+}, and does not suffer a decrease in melting temperature or change in oligomerization state relative to the wild type (*58*), suggesting that the functional differences of the triple mutant are, in fact, due to the specific altering of a binding event by one or more of the three side chain mutations. To examine the relative contributions of each of the three mutations, we created the three single mutants and conducted yeast two-hybrid assays for the interaction of each with Jab1. We determined that each of the

three single mutations significantly weakens the S100A7−Jab1 interaction relative to that of wild-type S100A7, and to a degree that is similar to the overall effect of the triple mutant $S100A7_3$ (Figure 5). While Asp56Gly shows the strongest effect, the Leu78Met mutation that is directly adjacent to the ANS binding site is also strong despite the conservative nature of this hydrophobic-for-hydrophobic mutation. Two copies of Leu78 line the hydrophobic gorge along the C_2 axis of the S100A7 homodimer, and the binding of 2,6-ANS to S100A7 causes each monomer's neighboring Met12 residue to undergo a well-ordered reorientation that significantly alters the shape of the continuous hydrophobic Met12−Leu78 recognition surface. In the absence of an S100A7 costructure with any of its protein binding partners, we cannot speculate in any detail about the orientations of Met12 and Leu78 that might be adopted in the complexes, but all of this evidence, taken together, leads us to propose that the Met12 cleft discovered in this study due to its occupation by ANS is relevant to one or more of the physiologically relevant complexes formed by S100A7.

The importance of S100 proteins as signaling proteins with tissue- and pathology-specific distributions is increasing, but few examples of small molecule binding have been reported for any members of this family (*35*−*39*). Among S100 proteins, S100A7 is typical in its lack of mutation and structural data relating to functions and formation of complexes. The demonstration of the Met12 cleft as a small molecule binding site with the potential also to be a protein−protein binding site is an important step in understanding and inhibiting protein−protein complexes of S100A7. We are currently using these data to pursue small molecules that report on and modify the interaction of S100A7 with Jab1.

ACKNOWLEDGMENT

We thank Melanie Olsen for the contribution of the S100A7 plasmid.

REFERENCES

1. Marenholz, I., Heizmann, C. W., and Fritz, G. (2004) S100 proteins in mouse and man: From evolution to function and pathology (including an update of the nomenclature). *Biochem. Biophys. Res. Commun. 322*, 1111–1122.
2. Engelkamp, D., Schafer, B. W., Mattei, M. G., Erne, P., and Heizmann, C. W. (1993) Six S100 genes are clustered on human chromosome 1q21: Identification of two genes coding for the two previously unreported calcium-binding proteins S100D and S100E. *Proc. Natl. Acad. Sci. U.S.A. 90*, 6547–6551.
3. Schafer, B. W., Wicki, R., Engelkamp, D., Mattei, M. G., and Heizmann, C. W. (1995) Isolation of a YAC clone covering a cluster of nine S100 genes on human chromosome 1q21: Rationale for a new nomenclature of the S100 calcium-binding protein family. *Genomics 25*, 638–643.
4. Sturchler, E., Cox, J. A., Durussel, I., Weibel, M., and Heizmann, C. W. (2006) S100A16, a novel calcium-binding protein of the EF-hand superfamily. *J. Biol. Chem. 281*, 38905–38917.
5. Madsen, P., Rasmussen, H. H., Leffers, H., Honore, B., Dejgaard, K., Olsen, E., Kiil, J., Walbum, E., Andersen, A. H., and Basse, B.; et al. (1991) Molecular cloning, occurrence, and expression of a novel partially secreted protein "psoriasin" that is highly up-regulated in psoriatic skin. *J. Invest. Dermatol. 97*, 701–712.
6. Boniface, K., Bernard, F.-X., Garcia, M., Gurney, A. L., Lecron, J.-C., and Morel, F. (2005) IL-22 Inhibits Epidermal Differentiation and Induces Proinflammatory Gene Expression and Migration of Human Keratinocytes. *J. Immunol. 174*, 3695–3702.
7. Boniface, K., Diveu, C., Morel, F., Pedretti, N., Froger, J., Ravon, E., Garcia, M., Venereau, E., Preisser, L., Guignouard, E., Guillet, G., Dagregorio, G., Pene, J., Moles, J.-P., Yssel, H., Chevalier, S., Bernard, F.-X., Gascan, H., and Lecron, J.-C. (2007) Oncostatin M Secreted by Skin Infiltrating T Lymphocytes Is a Potent Keratinocyte Activator Involved in Skin Inflammation. *J. Immunol. 178*, 4615–4622.
8. Wolf, R., Howard, O. M. Z., Dong, H.-F., Voscopoulos, C., Boeshans, K., Winston, J., Divi, R., Gunsior, M., Goldsmith, P., Ahvazi, B., Chavakis, T., Oppenheim, J. J., and Yuspa, S. H. (2008) Chemotactic Activity of S100A7 (Psoriasin) Is Mediated by the Receptor for Advanced Glycation End Products and Potentiates Inflammation with Highly Homologous but Functionally Distinct S100A15. *J. Immunol. 181*, 1499–1506.
9. Glaser, R., Harder, J., Lange, H., Bartels, J., Christophers, E., and Schroder, J.-M. (2005) Antimicrobial psoriasin (S100A7) protects human skin from *Escherichia coli* infection. *Nat. Immunol. 6*, 57.
10. Lee, K. C., and Eckert, R. L. (2006) S100A7 (Psoriasin): Mechanism of Antibacterial Action in Wounds. *J. Invest. Dermatol. 127*, 945.
11. Zhang, H., Zhao, Q., Chen, Y., Wang, Y., Gao, S., Mao, Y., Li, M., Peng, A., He, D., and Xiao, X. (2008) Selective expression of S100A7 in lung squamous cell carcinomas and large cell carcinomas but not in adenocarcinomas and small cell carcinomas. *Thorax 63*, 352–359.
12. Celis, J. E., Rasmussen, H. H., Vorum, H., Madsen, P., Honore, B., Wolf, H., and Orntoft, T. F. (1996) Bladder squamous cell carcinomas express psoriasin and externalize it to the urine. *J. Urol. 155*, 2105–2112.
13. Ralhan, R., DeSouza, L. V., Matta, A., Chandra Tripathi, S., Ghanny, S., Datta Gupta, S., Bahadur, S., and Siu, K. W. M. (2008) Discovery and Verification of Head-and-neck Cancer Biomarkers by Differential Protein Expression Analysis Using iTRAQ Labeling, Multidimensional Liquid Chromatography, and Tandem Mass Spectrometry. *Mol. Cell. Proteomics 7*, 1162–1173.
14. Webb, M., Emberley, E. D., Lizardo, M., Alowami, S., Qing, G., Alfia'ar, A., Snell-Curtis, L. J., Niu, Y., Civetta, A., Myal, Y., Shiu, R., Murphy, L. C., and Watson, P. H. (2005) Expression analysis of the mouse S100A7/psoriasin gene in skin inflammation and mammary tumorigenesis. *BMC Cancer 5*, 17.
15. El-Rifai, W., Moskaluk, C. A., Abdrabbo, M. K., Harper, J., Yoshida, C., Riggins, G. J., Frierson, H. F.Jr., and Powell, S. M. (2002) Gastric cancers overexpress S100A calcium-binding proteins. *Cancer Res. 62*, 6823–6826.
16. Brouard, M. C., Saurat, J. H., Ghanem, G., and Siegenthaler, G. (2002) Urinary excretion of epidermal-type fatty acid-binding protein and S100A7 protein in patients with cutaneous melanoma. *Melanoma Res. 12*, 627–631.
17. Moog-Lutz, C., Bouillet, P., Regnier, C. H., Tomasetto, C., Mattei, M. G., Chenard, M. P., Anglard, P., Rio, M. C., and Basset, P. (1995) Comparative expression of the psoriasin (S100A7) and S100C genes in breast carcinoma and co-localization to human chromosome 1q21-q22. *Int. J. Cancer 63*, 297–303.
18. Enerback, C., Porter, D. A., Seth, P., Sgroi, D., Gaudet, J., Weremowicz, S., Morton, C. C., Schnitt, S., Pitts, R. L., Stampl, J., Barnhart, K., and Polyak, K. (2002) Psoriasin expression in mammary epithelial cells in vitro and in vivo. *Cancer Res. 62*, 43–47.
19. Leygue, E., Snell, L., Hiller, T., Dotzlaw, H., Hole, K., Murphy, L. C., and Watson, P. H. (1996) Differential expression of psoriasin messenger RNA between in situ and invasive human breast carcinoma. *Cancer Res. 56*, 4606–4609.
20. Mandal, S., Curtis, L., Pind, M., Murphy, L. C., and Watson, P. H. (2007) S100A7 (psoriasin) influences immune response genes in human breast cancer. *Exp. Cell Res. 313*, 3016–3025.
21. Santamaria-kisiel, L., Rintala-dempsey, A. C., and Shaw, G. S. (2006) Calcium-dependent and -independent interactions of the S100 protein family. *Biochem. J. 396*, 201–214.
22. Emberley, E., Gietz, R. D., Campbell, J. D., HayGlass, K., Murphy, L., and Watson, P. (2002) RanBPM interacts with psoriasin in vitro and their expression correlates with specific clinical features in vivo in breast cancer. *BMC Cancer 2*, 28.
23. Ruse, M., Lambert, A., Robinson, N., Ryan, D., Shon, K. J., and Eckert, R. L. (2001) S100A7, S100A10, and S100A11 Are Transglutaminase Substrates. *Biochemistry 40*, 3167–3173.
24. Hagens, G., Masouyé, I., Augsburger, E., Hotz, R., Saurat, J. H., and Siegenthaler, G. (1999) Calcium-binding protein S100A7 and epidermal-type fatty acid-binding protein are associated in the cytosol of human keratinocytes. *Biochem. J. 339*, 419–427.
25. Ruse, M., Broome, A.-M., and Eckert, R. L. (2003) S100A7 (Psoriasin) Interacts with Epidermal Fatty Acid Binding Protein and Localizes in Focal Adhesion-Like Structures in Cultured Keratinocytes. *J. Invest. Dermatol. 121*, 132–141.
26. Emberley, E. D., Niu, Y., Leygue, E., Tomes, L., Gietz, R. D., Murphy, L. C., and Watson, P. H. (2003) Psoriasin Interacts with Jab1 and Influences Breast Cancer Progression. *Cancer Res. 63*, 1954–1961.

27. Emberley, E. D., Niu, Y., Curtis, L., Troup, S., Mandal, S. K., Myers, J. N., Gibson, S. B., Murphy, L. C., and Watson, P. H. (2005) The S100A7-c-Jun Activation Domain Binding Protein 1 Pathway Enhances Prosurvival Pathways in Breast Cancer. *Cancer Res. 65*, 5696–5702.
28. Emberley, E. D., Alowami, S., Snell, L., Murphy, L. C., and Watson, P. H. (2004) S100A7 (psoriasin) expression is associated with aggressive features and alteration of Jab1 in ductal carcinoma in situ of the breast. *Breast Cancer Res. 6*, R308–R315.
29. Paruchuri, V., Prasad, A., McHugh, K., Bhat, H. K., Polyak, K., and Ganju, R. K. (2008) S100A7-Downregulation Inhibits Epidermal Growth Factor-Induced Signaling in Breast Cancer Cells and Blocks Osteoclast Formation. *PLoS ONE 3*, e1741.
30. Wang, J., Barnes, R., West, N., Olson, M., Chu, J., and Watson, P. (2008) Jab1 is a target of EGFR signaling in ERα-negative breast cancer. *Breast Cancer Res. 10*, R51.
31. Jinquan, T., Vorum, H., Larsen, C., Madsen, P., Rasmussen, H., Gesser, B., Etzerodt, M., Honoré, B., Celis, J., and Thestrup-Pedersen, K. (1996) Psoriasin: A novel chemotactic protein. *J. Invest. Dermatol. 107*, 5–10.
32. Jiang, W. G., Watkins, G., Douglas-Jones, A., and Mansel, R. E. (2004) Psoriasin is aberrantly expressed in human breast cancer and is related to clinical outcomes. *Int. J. Oncol. 25*, 81–85.
33. Brodersen, D. E., Etzerodt, M., Madsen, P., Celis, J. E., Thogersen, H. C., Nyborg, J., and Kjeldgaard, M. (1998) EF-hands at atomic resolution: The structure of human psoriasin (S100A7) solved by MAd phasing. *Structure 6*, 477–489.
34. Brodersen, D. E., Nyborg, J., and Kjeldgaard, M. (1999) Zinc-binding site of an S100 protein revealed. Two crystal structures of Ca^{2+}-bound human psoriasin (S100A7) in the Zn^{2+}-loaded and Zn^{2+}-free states. *Biochemistry 38*, 1695–1704.
35. Markowitz, J., Chen, I., Gitti, R., Baldisseri, D. M., Pan, Y., Udan, R., Carrier, F., MacKerell, A. D.Jr., and Weber, D. J. (2004) Identification and characterization of small molecule inhibitors of the calcium-dependent S100B-p53 tumor suppressor interaction. *J. Med. Chem. 47*, 5085–5093.
36. Zhong, S., Macias, A. T., and MacKerell, A. D.Jr. (2007) Computational identification of inhibitors of protein-protein interactions. *Curr. Top. Med. Chem. 7*, 63–82.
37. Garrett, S. C., Hodgson, L., Rybin, A., Toutchkine, A., Hahn, K. M., Lawrence, D. S., and Bresnick, A. R. (2008) A biosensor of S100A4 metastasis factor activation: Inhibitor screening and cellular activation dynamics. *Biochemistry 47*, 986–996.
38. Charpentier, T. H., Wilder, P. T., Liriano, M. A., Varney, K. M., Pozharski, E., MacKerell, A. D.Jr., Coop, A., Toth, E. A., and Weber, D. J. (2008) Divalent Metal Ion Complexes of S100B in the Absence and Presence of Pentamidine. *J. Mol. Biol. 382*, 56.
39. Charpentier, T. H., Wilder, P. T., Liriano, M. A., Varney, K. M., Zhong, S., Coop, A., Pozharski, E., Alexander, D., MacKerell, J., Toth, E. A., and Weber, D. J. (2009) Small Molecules Bound to Unique Sites in the Target Protein Binding Cleft of Calcium-Bound S100B As Characterized by Nuclear Magnetic Resonance and X-ray Crystallography. *Biochemistry 48*, 6202–6212.
40. Slavik, J. (1982) Anilinonaphthalene sulfonate as a probe of membrane composition and function. *Biochim. Biophys. Acta 694*, 1–25.
41. Ke, S., Wright, J. C., and Kwon, G. S. (2007) Avidin-biotin-PEG-CPA complexes as potential EPR-directed therapeutic protein carriers: Preparation and characterization. *Bioconjugate Chem. 18*, 1644–1650.
42. Chaves, J. M., Srivastava, K., Gupta, R., and Srivastava, O. P. (2008) Structural and functional roles of deamidation and/or truncation of N- or C-termini in human αA-crystallin. *Biochemistry 47*, 10069–10083.
43. Hawe, A., Sutter, M., and Jiskoot, W. (2008) Extrinsic fluorescent dyes as tools for protein characterization. *Pharm. Res. 25*, 1487–1499.
44. Togashi, D. M., and Ryder, A. G. (2008) A fluorescence analysis of ANS bound to bovine serum albumin: Binding properties revisited by using energy transfer. *J. Fluoresc. 18*, 519–526.
45. Gasymov, O. K., and Glasgow, B. J. (2007) ANS fluorescence: Potential to augment the identification of the external binding sites of proteins. *Biochim. Biophys. Acta 1774*, 403–411.
46. Kirk, W., Kurian, E., and Wessels, W. (2007) Photophysics of ANS. V. Decay modes of ANS in proteins: The IFABP-ANS complex. *Biophys. Chem. 125*, 50–58.
47. Pflugrath, J. (1999) The finer things in X-ray diffraction data collection. *Acta Crystallogr. D55*, 1718–1725.
48. Collaborative Computational Project Number 4 (1994) The CCP4 Suite: Programs for protein crystallography. *Acta Crystallogr. D50*, 760–763.
49. Vagin, A., and Teplyakov, A. (1997) MOLREP: An Automated Program for Molecular Replacement. *J. Appl. Crystallogr.* 1022–1025.
50. Emsley, P., and Cowtan, K. (2004) Coot: Model-building tools for molecular graphics. *Acta Crystallogr. D60*, 2126–2132.
51. Murshudov, G. N., Vagin, A. A., and Dodson, E. J. (1997) Refinement of macromolecular structures by the maximum-likelihood method. *Acta Crystallogr. D53*, 240–255.
52. Gasymov, O. K., Abduragimov, A. R., and Glasgow, B. J. (2007) Evidence for internal and external binding sites on human tear lipocalin. *Arch. Biochem. Biophys. 468*, 15–21.
53. Bohne, C. R., and Scaiano, J. C. (1991) Photochemistry in Organized and Constrained Media , VCH Publishers, New York.
54. Gietz, R. D., and Schiestl, R. H. (2007) Quick and easy yeast transformation using the LiAc/SS carrier DNA/PEG method. *Nat. Protoc. 2*, 35–37.
55. Huang, J., and Bright, F. V. (1990) Unimodal Lorentzian Lifetime Distributions for the 2-Anilinonaphthalene-6-sulfonate−β-Cyclodextrin Inclusion Complex Recovered by Multifrequency Phase-Modulation Fluorometry. *J. Phys. Chem. 94*, 8457–8463.
56. Kirk, W. R., Kurian, E., and Prendergast, F. G. (1996) Characterization of the sources of protein-ligand affinity: 1-Sulfonato-8-(1′)anilinonaphthalene binding to intestinal fatty acid binding protein. *Biophys. J. 70*, 69–83.
57. Gasymov, O. K., Abduragimov, A. R., and Glasgow, B. J. (2008) Ligand binding site of tear lipocalin: Contribution of a trigonal cluster of charged residues probed by 8-anilino-1-naphthalenesulfonic acid. *Biochemistry 47*, 1414–1424.
58. West, N. R., Farnell, B., Murray, J. I., Hof, F., Watson, P. H., and Boulanger, M. J. (2009) Structural and functional characterization of a triple mutant form of S100A7 defective for Jab1 binding. *Protein Sci.* (in press).